University of BRISTOL

SCHOOL OF PHYSICS

FINAL YEAR PROJECT REPORT

NAME:	Thomas Botwood
DEGREE COURSE:	Chemical Physics (Msci)
PROJECT TITLE:	Functionalised Diamond Surfaces
YEAR OF SUBMISSION:	2026
SUPERVISOR:	Neil Fox
NUMBER OF WORDS:	8372

Declaration

There are a few datapoints that were not collected by me. The data on the Boron dopant density of the P-type diamond deposition was provided by Liam Cullingford along with the code that acquired the electron gun data. Although I was present for much of it, the vast majority of the data acquisition from and operation of the NanoESCA equipment was done by Jude Laverock. He also used his Matlab script to generate the work function maps from the raw CCD data. All other data was taken and analysed by me unless otherwise specified. The two parts of manufacturing the diodes that were not done by me was the chromium coating that was done by Neil and the mlecular O_2 termaination that was done by Jude.

The theory that temperature could be affecting my diode when the electron gun was in use was first put forward by my supervisor Neil Fox, although I realised that resistance was decreasing with temperature and not increasing. It was also Jude that suggested the strange UPS spectra may be due to amorphous diamond. The growth times I used for the P-type and intrinsic layers of my devices were suggested by Neil and Ramiz Zulkharnay.

AI Declaration

No AI was used in this project except for spelling and grammar checking.

Acknowledgements

I would like to thank my supervisor Neil for his insight and continuous guidance throughout this project. I would also like to thank Liam for his training and direct help with the electron gun, in addition to supervision when I was not yet competent with the CVD reactors. I also need to thank Liam for his advice on research and presenting my findings. Ramiz was a great help in this project, as he trained me on the use of the CVD reactors and the UV ozone terminator. He also advised me on the design of my diodes and has been an amazing source of knowledge on the different methods of oxygen termination. Special thanks to Catherine the training on using the chromium etcher and finding my sample after it flicked out of my tweezers and I thought it was lost forever.

I would also like to thank Jude for his immense help and patience with the chaos that my data acquisition in the NanoESCA became. He always had great ideas for how I could interpret my data and what readings we could take next, even when the planned three-day acquisition became two weeks. I am indebted to James for sharing his knowledge of all the equipment in the lab and for always helping with every problem and strange issue this equipment has. He also deserves thanks for the training on Ramen spectroscopy and laser safety, and also spending ages chatting with me about uses for all the old equipment in the lab.

I am very grateful to my tutor Allen for his feedback on this report and his general advice on scientific writing. I of course have to thank all my fellow budgies in the diamond lab for always being happy to lend a hand and double-check my work. In particular, I must thank the fellow members of Neil's group Julia, Elâ, Sophie, Joe, Simran, and Sarah.

I would like to thank my mum for proofreading countless drafts of this report as I found new and groundbreaking ways to misspell the same word. I would also like to thank my dad for feeding me while I spend weeks hardly leaving the office trying to polish the report. My parents combined help with the grammar in this report Is what has made it human-readable.

Lastly I would like to thank my partner Beau. Even though the diamond lab is in the basement, I always felt a ray of sunshine whenever we could chat. I want to thank Beau for their continued support, their belief in me and for putting up with me filling their desk with textbooks when doing research.

Abstract

A P-type intrinsic metal Schottky diode was made by depositing layers of diamond using chemical vapour deposition. Two different oxygen termination methods were used before chromium plating to reduce the Schottky barrier height. XPS showed that the oxygen termination diffuses through the chromium layers, suggesting it has a minimal impact on the SBH and could negatively impact diode performance. The average work functions of the chromium and diamond were $4.21\,eV$ and $4.56\,eV$ respectively. After plasma etching, the diamond was found to be metal like using UPS. It was also found that heat has a negative effect on the diode's rectification.

1 Introduction

In the 21st century there appears to be a type of energy generation and storage for every application. For high power and low capacity there are supercapacitors[1]. If more capacity is required, there are lithium-ion batteries and lead acid batteries are still in use due to their high resiliency, low cost, and low leakage current[2, 3]. Furthermore, energy storage has been scaled up to help support the grid, with two examples being pumped hydro storage and flywheels[4]. However, there is a gap in capability that needs to be filled.

Currently, there are very few options for applications that require an extremely long life power source. Examples of these applications include deep space satellites, which require an energy source when too far from the sun for reliable solar power[5]; remote sensors and trackers, where connection to the power grid may be impossible and battery changes too infrequent for conventional energy storage[6]; and pacemakers, where access to the device is difficult and invasive[7].

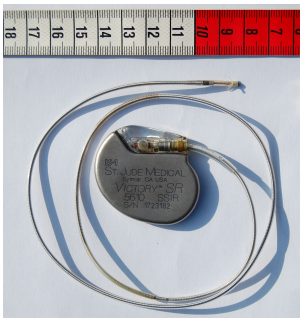

Figure 1: A photo of a Victory SR 5610 pacemaker powered by a chemical battery[8]. This model of pacemaker is expected to last 6.5 years[9].

Modern pacemakers use ultra long life chemical batteries, such as lithium iodide batteries. These batteries can last for up to ten years and are a well proven technology[7]. However, they are not ideal due to the difficulty and invasiveness of changing pacemaker batteries and the risk of complications[10]. Zinc air batteries are used for animal trackers, as they obtain the oxidiser from the atmosphere keeping them very lightweight[6]. These battery technologies are all limited by a short lifetime. Indeed, the limited lifetime of chemical batteries means they cannot be used in many applications such as satellites, where device lifetimes are measured in decades [11]. In these situations, it might be best to move from chemical energy storage to nuclear energy.

Some of the very first pacemakers used radioisotope thermoelectric generators (RTGs) for power. These devices use high activity radioisotopes such as P^{238} and Sr^{90} to generate heat creating a heat differential which can be directly converted into electrical power[13]. However, their use in pacemakers ceased when chemical replacements came on the market due to plutonium's toxicity, but their use in satellites continues[7]. Many satellites and rovers have used RTGs for power when sunlight isn't plentiful, such as for deep space missions far from the sun (for example, Voyager 2) or when the sun isn't visible due to clouds or shadows (for example, Curiosity). RTGs also have the advantage of a high power output, which will only reduce around 2% per year.

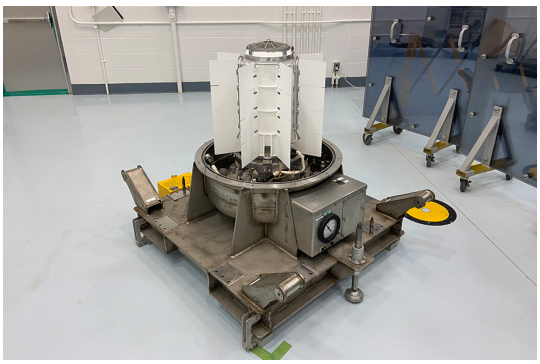

Figure 2: A radioisotope thermoelectric generator intended for spacecraft[12].

However, there are significant disadvantages to RTGs. Firstly, if a radioisotope's activity is high enough to generate heat, it is also very dangerous and requires plenty of shielding[14]. Furthermore, RTGs also have a very low efficiency of about 7% because they indirectly convert energy from radioactive decay to electricity via heat [15]. The problems of low efficiency and high activity sources compound to make the cost of a spaceflight capable RTG around a hundred million dollars [16].

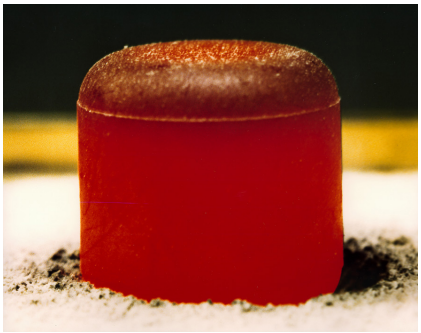

Figure 3: A plutonium-238 oxide RTG fuel pellet for the Cassini mission, glowing red from the alpha radiation[17].

A much improved counterpart to RGTs are betavoltaic cells. Like RTGs, betavoltaic cells harness the energy of radioisotopes, which allows the technology to have an extremely high energy density[18]. However, in contras to RTGs, betavoltaic cells directly convert radioactive decay particles into electrical energy, making the conversion far more efficient. This higher efficiency also means high activity radioisotopes are not required, improving lifetime, cost, and safety of the device. Furthermore, the lack of shielding and cooling fins that are required for RTGs make the device simpler and lighter. However, betavoltaic cells are not yet a mature technology and there may be many ways in which their efficiency can be increased that have not yet been explored.

In this project I have built P-type intrinsic metal (PIM) Schottky diodes that work as betavoltaic cells and researched their properties. These were made from both polycrystalline diamond (PCD) and single crystal diamond (SCD). Two different oxygen termination methods were used on the diamond before depositing the metal layer to lower the Schottky barrier height (SBH). This resulted in four different diodes that were then compared. These diodes were characterised using a number of techniques to assess their performance as betavoltaic cells. In the NanoESCA facility, XPS and a plasma etcher were used to identify each component of the intrinsic-metal interface and find their depth. This facility was also used to map the work function and Fermi level intensity around this interface. The energy generation capabilities of the cells were measured using an electron gun, simulating nuclear decay. These measurements were undertaken to investigate possible improvements to the efficiency of the device and lowering of the Schottky barrier height.

2 Background Theory

2.1 PIN Betavoltaic Cell

A betavoltaic cell is a power source that generates electricity from a beta radiation (high speed electrons) emitting isotopes using a P-N junction[19]. These devices are similar to a solar cell made with a P-type intrinsic N-type (PIN) diode. In the solar cell, photons interact with electrons in the intrinsic semiconducting region to promote them from the valence band to the conduction band, creating electron hole pairs[20]. Due to the band structure of the diode, the electrons flow to the P-type side creating a negative charge, and the holes flow to the N-type side creating a positive charge. In a diode, electrons cannot flow from P-type to N-type doped semiconductor, so instead the electrons have to flow around a current to balance out the charge, generating a current[21].

In a betavoltaic cell, the beta radiation takes the place of the photons in a solar cell by creating electron hole pairs in the intrinsic semiconducting region. There are some key differences though. In photovoltaics the energy of a single photon is much less than the energy of a beta particle. This means that for peak efficiency the semiconductor band gap (E_g) for a betavoltaic cell must be larger than the band gap in a solar cell[22]. This is because if the electron-hole pair is exited too far above the band gap, the excess energy is lost due to thermal relaxation[23]. Another difference with betavoltaics is that a single beta particle can create multiple electron hole pairs before it comes to a stop, thus reducing the efficiency penalty from using a semiconductor with a band gap significantly lower than particle energy[18]. This is in contrast to photovoltaic cells, where a single photon can only create one electron hole pair.

There are many unique aspects of using a betavoltaic cell as an energy source. One of them is that the power output is consistent over a very long period of time[24]. An ideal betavoltaic cell will have a power output proportional to the activity of the radiation source, so with the right isotope the battery can maintain much of its power output for tens or hundreds of years, depending on the isotope's half-life[18]. They also have a very high energy density ($10000\,Whkg^{-1}$), an advantage intrinsic to nuclear energy[25, 26].

The main disadvantage of betavoltaics is the very low power output, in the range of tens of microwatts, which is far too low for most applications[27]. For GPS receivers, even low power optimised devices have a power consumption many times higher than can be generated with current betavoltaics[28]. Until massive improvements can be made, the solution to this is to power more complicated circuits in short pulses from energy stored in a supercapacitor. Using this method, in conjunction with high quality components, a power hungry GPS module can send out a location ping every few hours. Even with the low power output, there are a few applications that betavoltaics can directly power in their current state such as medical devices, small satellites, and micro electrical mechanical systems (MEMS)[24, 26].

The high cost of nuclear material in betavoltaic cells is a significant barrier to their widespread adoption. Typical isotopes used as a beta radiation source include H^3, Sr^{90}, Y^{90}, Ni^{63}, and C^{14}[26, 29, 30]. The cost for some of these is very high, with the cost tritium (H^3) being over $\$25,000$ per gram and even the comparatively cheap irradiated graphene still needs to be refined, which itself is an expensive process[31, 32].

The final hurdle for the use of betavoltaics relate to the laws controlling the ownership and sale of nuclear material. According to British law, any reasonably sized beta emitter would be considered "in scope" nuclear material, which means it is controlled by the most stringent nuclear material regulations and therefore would require a permit to sell and store[33]. Getting these permits or licences can be slow and will therefore delay betavoltaic devices from coming to market[34]. These restrictions can also limit the amount of radioactive material used, and therefore the power output of the cells[22].

2.2 Semiconducting Diamond

The semiconductor used in my betavoltaic cells is diamond. Diamond is usually seen as an insulator, but insulators and conductors are only differentiated by the size of the band gap. At the energy scale of betavoltaics, diamond acts as a semiconductor. To make a useful device from a semiconductor it is necessary to dope it. P-type doped diamonds can be found in nature and were first discovered in 1952[35]. The reported properties that differentiated it from other diamonds were UV phosphorescence and a high conductivity[36]. This naturally doped diamond was boron doped diamond (BDD). This is the most common P-type diamond in use today due to its relatively shallow accepter level and high electron mobility[37]. For this reason it is the P-Type dopant used in this project.

The indirect band gap of diamond is $5.4\,eV$ and the smallest direct band gap is $7.3\,eV$. This corresponds to a photon wavelength of $230\,nm$ and $170\,nm$ respectively, which falls into the UVC band[38, 39]. While this is far lower than the average energy of a beta particle emitted from tritium or carbon-14 ($18.6\,keV$ and $50\,keV$ respectively), it is much larger than the band gap of other semiconductors, allowing a more efficient absorption of beta radiation[40, 41].

Another advantage of the use of diamond in betavoltaic cells is that it is a very radiation hard material, experiencing only insignificant changes in properties after a very large dose of radiation[42]. When compared to other semiconductors, such as silicon, diamond is two to three times more radiation hard[43]. Furthermore, diamond is very physically hard and strong, being many times harder than other semiconductors[44]. This reduces the risk of damage to the cell. Diamond is also stable at very high temperatures, allowing the cell to exist in extreme environments[44].

An additional reason to use diamond is the ability to incorporate the beta radiation source with the cell, as carbon-14 is a beta emitter[41]. By having the cell and carbon-14 be one contiguous diamond, it becomes difficult if not near impossible to isolate the radioactive material, lowering the chance of misuse by bad actors. This reduces the risk of legal liability and can make it easier to get the device registered[33]. Carbon-14 can be acquired from reprocessing irradiated graphite (i-graphite) waste sourced from graphite moderated nuclear reactors[45]. The UK alone had $86,000$ tons of i-graphite as of 2014, meaning there is plenty for mass production[46].

Conversely, a major disadvantage with using diamond as a semiconductor is the fact that there is no viable N-type dopant diamond. N-type diamond usually has low electrical quality and often suffers from uneven doping and lattice damage[47]. It took until the late 90's for any N-type diamond that could conduct at room temperature to be synthesised by adding phosphorous to the reactor when growing the diamond[48]. Other possible N-type dopants have been found to be inviable for a number of reasons; nitrogen doped diamond doesn't conduct at room temperature due to a high activation energy, and lithium ions irrevocably damage the diamond's structure[49]. Diamond betavoltaics are therefore limited to PIM (P-type Intrinsic Metal) cells, which are Schottky diodes. Unfortunately, Schottky diodes have a major disadvantage compared to conventional diodes, specifically the much higher leakage current[50]. This leakage current would usually be insignificant, but as betavoltaics have a very small current output of around $1\,\mu A$, this leakage current is proportionally a much larger problem[51].

2.3 Conventional and Schottky Diodes

In an extrinsic semiconductor, dopants add electron donors at an energy (E_D) just below the conduction band (N-Type) or, for electron accepters (E_A), just above the valence band (P-Type). Due to thermal excitation, these electrons and holes are promoted into their respective bands[52]. The density of ionised donors (N_D^+) and accepters (N_A^-) relates to the unionized concentrations of the dopants (N_D and N_A) and temperature (T) following the equations 1 and 2 respectively.

$$N_D^+ = \frac{N_D}{1 + g_D e^{(E_F - E_D)/k_b T}} \tag{1}$$

$$N_A^- = \frac{N_A}{1 + g_A e^{(E_A - E_F)/k_b T}} \tag{2}$$

Where k_b is Boltzmann's constant, E_F is the Fermi level and g is the ground state degeneracy, which is two for donors and four for accepters[52]. In most conventional semiconductors dopants are almost fully ionized at room temperature, therefore for most calculations we use the approximations $N_D^+ \approx N_D$ and $N_A^- \approx N_A$. This lack of control of the density of conducting particles is a great improvement over the carrier concentration in intrinsic semiconductors, shown in the following equations:

$$n = N_C \exp\left(-\frac{E_C - E_F}{k_b T}\right) \tag{3}$$

$$p = N_V \exp\left(-\frac{E_F - E_V}{k_b T}\right) \tag{4}$$

Where n and p is the negative and positive charge carrier density, N_C and N_V is the density of states in the conduction and valence band, E_C is the energy levels of the bottom of the conduction band, and E_V is the energy levels of the top of the valence band.

The aforementioned band structure of a diode is formed by the excess electrons in the N-type semiconductor flowing into the P-type semiconductor and the excess holes in the P-type semiconductor flowing into the N-type semiconductor[53]. This diffusion continues until the Fermi level is completely flat, creating a charge distribution across the junction, shown in figure 4. It is this charge distribution that bends the electronic bands.

The depletion widths in the N-type and P-type sides of the junction (x_n and x_p) can be found using the following equations:

$$x_n = \sqrt{\frac{2\epsilon_s V_{bi}}{q} \frac{N_A}{N_D(N_A + N_D)}} \tag{5}$$

$$x_p = \sqrt{\frac{2\epsilon_s V_{bi}}{q} \frac{N_D}{N_A(N_A + N_D)}} \tag{6}$$

Where q is the charge of an electron, ϵ_s is the permittivity in the semiconductor, and V_{bi} is the built-in voltage.

The built-in voltage is created by the charge distribution and can be calculated using the following equation:

$$qV_{bi} = E_g - \zeta_n - \zeta_p \tag{7}$$

Where E_g is the band gap, ζ_n is the difference between the conduction band and Fermi level (E_F)in the N-type

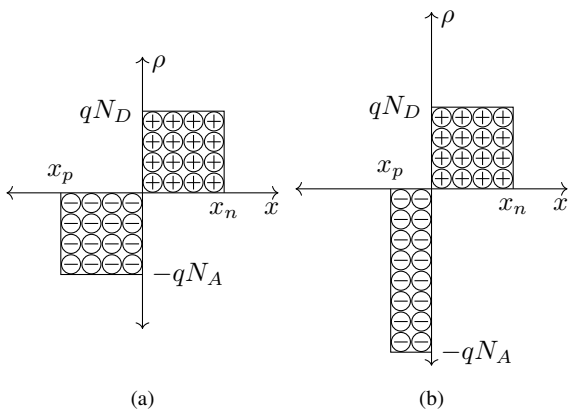

Figure 4: Two diagrams showing the space-charge distribution at a PN junction demonstrating the overall neutral charge and the relationship between dopant density (N) and depletion width (x). The two scenarios shown are when (a) accepter and donor density are the same and (b) when accepter density is higher that donor density.

semiconductor and ζ_p is the difference between the Fermi level and the valence band in the P-type semiconductor. To find the Fermi energy (E_F) of an extrinsic semiconductor we can assume that most charge carriers in an extrinsic semiconductor are from doping, and therefore we can assume that equations 1 and 2 are roughly equal to equations 3 and 4 respectively. This assumption gives us the following equations:

$$N_C \exp\left(-\frac{E_C - E_F}{k_b T}\right) \approx \frac{N_D}{1 + g_D e^{(E_F - E_D)/k_b T}} \tag{8}$$

$$N_V \exp\left(-\frac{E_F - E_V}{k_b T}\right) \approx \frac{N_A}{1 + g_A e^{(E_A - E_F)/k_b T}} \tag{9}$$

Which can be solved to find the Fermi energy.

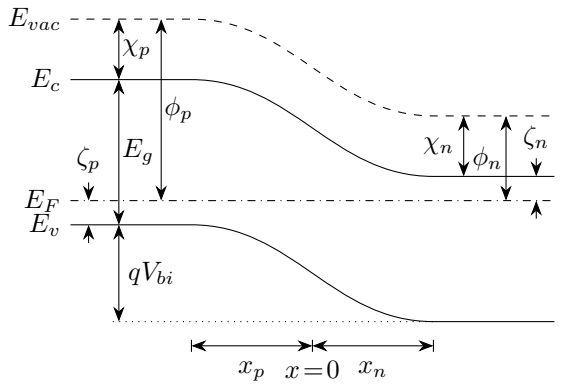

Figure 5: A diagram of the band structure of a PN junction with the P-type semiconductor on the left, the N-type semiconductor on the right, and the interface at $x = 0$.

Bands bend a little differently in a Schottky diode when compared to a conventional diode. In a Schottky diode there is an intrinsic semiconductor and a metal and, much like a PN junction, the Fermi energy in the semiconductor will move to match the Fermi energy in the metal. This will create a charge distribution inside the semiconductor that bends the bands and creates a barrier in energy between the Fermi level in the metal and the conducting band in the semiconductor[52]. This barrier can be calculated using the work functions of the metal and semiconductor (ϕ_m), and the electron affinity of the semiconductor ($\chi_{n/p}$).

The work function of a material is the amount of energy it takes to remove an electron from its surface[54]. When modelling semiconductors the requirement of the electron being removed from the surface is ignored, making it possible to model the bulk of the material. In these situations the work function is defined as the difference in energy between the vacuum level and the Fermi level. The electron affinity is similarly defined as the difference in energy between the vacuum level and the conduction band.

At the metal-semiconductor interface all charge carriers in the metal are ϕ_m below the vacuum level. This charge distribution bends the bands in the semiconductor until the semiconductor work function at the interface is the same as the metal work function. However, the charge distribution doesn't change the electron affinity (as shown in figure 5) and therefore the barrier charge carriers have to overcome is defined by the following equations:

$$\phi_{Bn} = \phi_m - \chi_n \tag{10}$$

$$\phi_{Bp} = E_g - (\phi_m - \chi_p) \tag{11}$$

Where ϕ_{Bn} and ϕ_{Bp} are the Schottky barrier heights for N-type and P-type semiconductors respectively. This barrier is shown in figure 6.

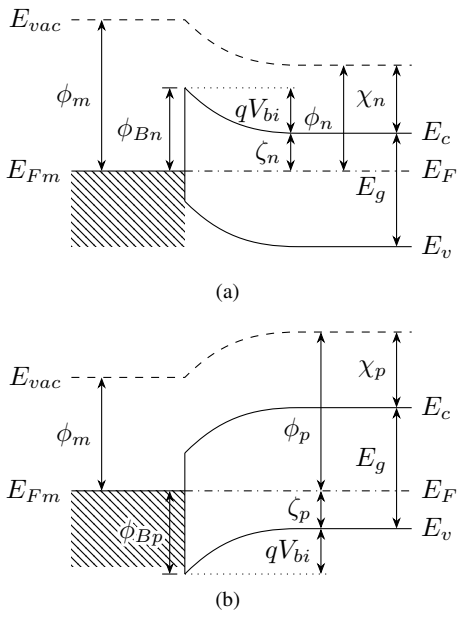

Figure 6: A diagram of the band structure of a Schottky junction with an (a) N-type semiconductor and a (b) P-type

The depletion region inside the semiconductor of a Schottky junction can be found using the following equation:

$$x_{n/p} = \sqrt{\frac{2\epsilon_s}{qN_{D/A}}\left(V_{bi} - \frac{k_bT}{q}\right)} \tag{12}$$

Using figure 6 it is also clear that the built-in voltage in a Schottky diode is:

$$qV_{bi} = \phi_B - \zeta \tag{13}$$

For both N and P-type Schottky diodes. Because the charge carrier density in a metal is significantly higher than in a semiconductor, the depletion region inside the metal of a Schottky diode is so small it is considered insignificant and is therefore not calculated.

2.4 Diamond CVD

Natural diamonds formed on earth originate in the upper mantle or in meteor impacts, where there is a very high temperature and high pressure environment[55]. These conditions are replicated by the high pressure high temperature (HPHT) technique for manufacturing diamonds to create conditions where the sp^3 form of carbon is the dominant phase[56]. This method was the main way of producing diamonds until the 1980s and was commonly used for mechanical applications such as for lapping grit and in jewellery.[57] However, the lack of control of crystal size and material shape using HPHT means a different technique is needed for other potential applications of diamond[58, 59].

Chemical Vapour Deposition (CVD) is when a material is grown on a hot surface from reactants in the gas phase[60]. Using CVD to deposit diamond thin films was first described in a 1962 patent where a seed crystal of diamond (substrate) was heated in a methane atmosphere, growing both diamond and graphite[61]. The patent claimed that the reason for any diamond growth instead of the much more stable graphite was because the reversible reaction between the diamond and methane "reaches equilibrium faster", something that is now known to be false. This misunderstanding of the process meant that a significant amount of graphite was still deposited, so the end product had little use[62].

Adding hydrogen to the gas mixture was found to be the solution to this issue, as it would preferentially etch away the graphite over the diamond[63]. Over time this repeated deposition and etching of carbon will slowly grow a diamond film as the graphite is etched away faster than it can be grown. This allows for very controlled growth of high purity polycrystalline and single crystal diamond. it is also possible to grow layers of doped diamond by adding a gaseous compound containing the dopant to the chamber. Diamond CVD requires a vacuum capable chamber that can dissipate heat fast. Inside this chamber there needs to be a method for heating up the substrate as well as the gas just above it. There are many different diamond CVD techniques that all aim to achieve similar conditions required for diamond growth[59]. The technique I've used to create the betavoltaic cell is Microwave Plasma CVD.

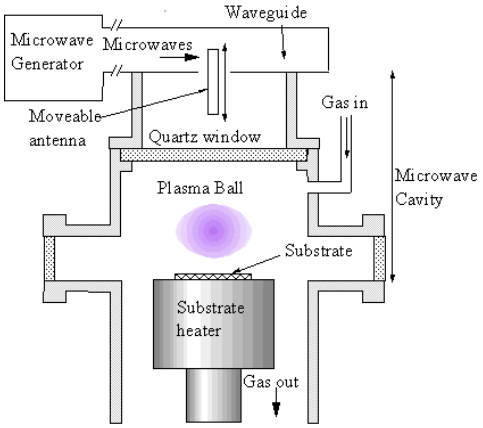

Figure 7: A diagram of the type of diamond microwave CVD reactor used in this project[64].

In Microwave Plasma CVD, a high power microwave source is focused onto the growth substrate. This creates a sufficient energy density to maintain a ball of plasma just above the substrate, which both heats up the substrate and the gas, allowing diamonds to grow[65]. The microwave antenna is moved and the shape of the waveguide is altered to focus the plasma ball. This allows the plasma ball to be kept away from the walls of the chamber, protecting the chamber walls from the heat and corrosiveness of the plasma. It also allows the substrate and gas to be heated separately by changing the height of the plasma ball. A diagram of the specific reactor design used in this project is shown in figure 7.

2.5 The Schottky Barrier Height and Oxygen Termination

The Schottky barrier is the feature in a Schottky diode that rectifies current. Its height directly corresponds to both the ability of the diode to rectify, reverse leakage current, and the forward bias resistance[66]. To tune these properties for a specific application, the Schottky barrier height (SBH) can be easily changed[67]. The work function and electron affinity are highly dependent on the surface/interface of the metal/semiconductor, and therefore so is the SBH. By terminating the surface of the diamond before adding the metal, we can achieve an ideal SBH for our device.

Hydrogen and oxygen termination change the work function and electron affinity of both doped and undoped diamond[68]. The oxygen termination for diamond is especially important as unterminated and hydrogen terminated diamond have a negative electron affinity. This means that, referring back to equation 10, the SBH of an N-type Schottky diode would be much larger than an optimal SBH. Oxygen terminated diamond has a positive electron affinity and therefore does not have this problem. So, by oxygen terminating the diamond the performance of the diode could be significantly improved.

Different types of oxygen termination can have varied effects on election affinity and work function[69]. This is because these techniques do not have the same levels of coverage and can form different species of oxygen. In my devices, two kinds of oxygen coating techniques were used: UV ozone oxygen coating and a relatively new molecular O_2 method that uses heat to desorb surface species and then exposes the surface to pure oxygen[70].

2.6 Betavoltaic Cell Design

The cells described in this report were grown in layers on top of an intrinsic diamond substrate. The ohmic contact was preserved by masking the end of wafer with a piece of diamond before depositing the intrinsic and metal layers. A top down and side view diagram of the devices can be seen in figure 8. The thickness of the P-type BDD should be $\sim 2\,\mu m$, the intrinsic diamond layer should be $\sim 6\,\mu m$, and the chromium plating is $\sim 80\,nm$.

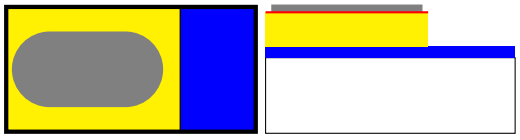

(a) (b)

Figure 8: A (a) top down and (b) side view of the betavoltaic cell design. White is the pre-made intrinsic diamond substrate, blue is the P-type BDD, yellow is intrinsic diamond, gray is chromium, and red is a layer of oxygen termination.

Figure 9 shows how the band structure changes through the diode. To find the depletion widths we first need to find the carrier densities. The boron concentration in the P-type layer is $\sim 5 \times 10^{21}\,cm^{-3}$ and usually we would assume the boron to completely ionise, but as the energy level of boron in diamond is fairly deep ($E_A - E_F = 0.373\,eV$) we have to use equation 2 to find N_A^-[71]. Using the assumption that $T = 298\,K$ $(25°C)$, I calculated that $N_A^- \approx 6.14 \times 10^{14}$. All following calculations were done assuming the same temperature.

To find the built-in voltage (V_{bi}) for the P-type - intrinsic junction we need the Fermi level position in both materials. For intrinsic diamond we can assume E_F to be in the centre of the band gap ($\zeta_i = E_F - E_V = 2.7\,eV$) but for P-type we have to solve equation 9 for E_F using the approximation $N_V \approx 10^{19}\,cm^{-3}$[72]. I found E_F had moved down $\sim 1.2\,eV$ meaning $\zeta_p = E_V - E_F \approx 1.5\,eV$. Using equation 7 it was calculated that $qV_{bi} = 1.2\,eV$.

To find the depletion widths at the P-type - intrinsic junction the carrier density of both materials must be known. The carrier density in the intrinsic material can be assumed to be the undoped electron density in the conduction band n, which can be calculated using equation 3. Using this equation and the density of states in the conduction band $N_C \approx 10^{20}$ I calculated that $n = 2 \times 10^{-26}\,cm^{-3}$. Using equations 5 and 6 with the substitutions $N_A = N_A^-$ and $N_D = n$ I calculated $x_p \approx 1.6 \times 10^{-27}\,m$ and $x_i \approx 1.9 \times 10^{14}$ (relative permittivity $\epsilon_r = 5.7$)[73]. Given these are respectively much smaller and larger than physically possible, it is clear that the P-type-intrinsic and intrinsic-chromium junctions cannot be modelled in isolation.

The electron affinity of undoped diamond is $-1.1\,eV$ for a clean surface and $1.9\,eV$ after oxygen termination. Using equation 11 and given that the work function of chromium is $4.6\,eV$, the theoretical barrier heights (ϕ_{Bp}) were found to be $-0.2\,eV$ and $2.8\,eV$ for clean and oxygen terminated diamond respectively[74]. Due to how deep the depletion of the P-type intrinsic junction is into the intrinsic semiconductor, we can assume the effective Fermi energy at the intrinsic-metal interface is the same as in the P-type material. Therefore, we can use the assumption that $\zeta \approx \zeta_p$ and equation 13 to find that $qV_{bi} = -1.7\,eV$ and $1.3\,eV$ for clean and oxygen terminated diamond respectfully. When calculating built-in voltage for a P-type Schottky junction, a negative V_bi means the junction will act more like an N-type junction as shown in figure 6a. The positive built-in voltage for the junction when using oxygen termination allows for a conventional P-type Schottky junction as shown in figure 6b. This is preferred as it allows the holes to flow directly to the P-type side of the junction.

2.7 Characterisation Techniques

The first instrument used to characterise the cells is the LEXT Confocal Laser Scanning Microscope. This is an optical microscope that can capture image data at different focus points and combine them so the entire image is in focus. It also uses a laser to create a height map of the sample. This is done by moving the focal point of the laser up and down. The intensity of the reflected laser light will reach a maximum when the focal point is at the surface. Multiples of these images and height maps can be taken at precise positions using the motorised stage and stitched together.

Most of the characterisation of the betavoltaic cells was done in the NanoESCA system. This system contains one chamber that has XPS and a plasma etcher. The plasma etcher slowly removes chromium from the surface nanometres at a time, while the XPS continuously captures spectra in specific binding energy ranges where components of interest have features. This means the composition of the material can be measured as a function of depth for many slices of a sample. This also allows the position of the components of the diode around the chromium interface to be identified.

The main measurement instrument in the NanoESCA system is energy-filtered photoelectron emission microscopy (EF-PEEM). This operates by ejecting electrons from the surface of the sample by UV photoemission. These electrons are filtered by energy and focused by two charged hemispheres onto a charged coupled device (CCD) giving a 2D array of electron energy spectrums.

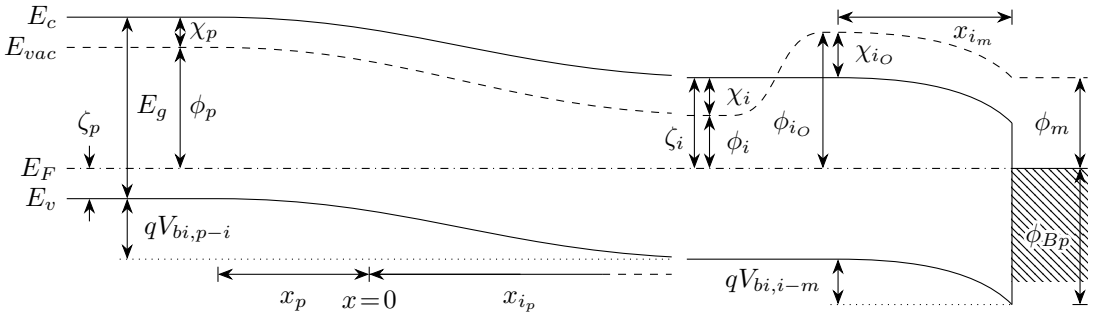

Figure 9: A band diagram showing the bending of the bands in the betavoltaic cells. Left to right there is P-type BDD, intrinsic diamond, oxygen terminated intrinsic diamond, and chromium. As electron hole pairs are generated by beta particles in the intrinsic section, electrons flow to the chromium and holes flow to the BDD.

This can be used to generate a map of the work function and Fermi level intensity. By using an unfocused beam, a UPS spectrum of the full image can be also be taken. These measurements were taken at both the etched and unetched area of the samples to compare the results of the intrinsic diamond and chromium coating.

The final characterisation was done using an electron gun to simulate the betavoltaic cell being exposed to beta radiation. This is done in a vacuum chamber to avoid the electrons being absorbed into the air.

3 Experimental

Semiconducting diamond was grown on SCD and PCD substrates acquired from Element 6. The two SCD substrates were used as is. These substrates had dimensions of $6.8\,mm \times 3.3\,mm \times 0.2\,mm$ and the face orientation was 110. The PCD originally had dimensions $10\,mm \times 10\,mm \times 0.5\,mm$. This substrate was diced using a laser cutter into two PCD substrates that were the same length and width as the SCD substrates.

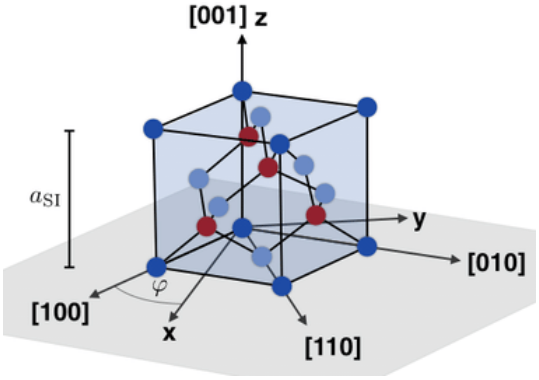

Figure 10: Diagram of a diamond unit cell with crystal directions labelled[75].

A layer of BDD was grown on all four substrates. This growth was done for an hour at $130\,torr$ with hydrogen, methane, and diborane (the boron source) flowing into the chamber at $300\,sccm$, $12.5\,sccm$, and $0.7\,sccm$ respectively.

$2\,mm$ at the end of all the samples were masked off with another diamond film and an undoped, intrinsic diamond layer was grown on the unmasked section. This growth was done for three hours with the pressure at $130\,torr$, hydrogen flow at $300\,sccm$, and methane flow at $12.5\,sccm$.

One of each single crystal and polycrystalline sample was oxygen terminated using the molecular O_2 method in the NanoESCA facility. Both samples were loaded into the NanoESCA UHV chamber and annealed at 700 $^\circ C$ for one hour. After the samples had cooled for half an hour they were moved to a separate chamber where they were exposed to O_2 at a pressure of $0.01\,mbar$ for 5 minutes. These samples were then metal coated with $\sim 84\,nm$ chromium using evaporative coating.

After oxygen termination, both the molecular O_2 terminated samples were analysed using the LEXT Laser Scanning Microscope. A height map of the diodes was created and stitched images of the two diodes were taken.

The other two samples were oxygen coated using UV ozone. First the samples were hydrogen terminated in a CVD reactor for 5 minutes at $130\,torr$ with $300\,sccm$ of hydrogen. After the plasma was stopped the samples were kept in a hydrogen environment for a further 5 minutes. These samples, along with an intrinsic diamond test sample, were then put in a chamber where UV generated ozone flowed over them for half an hour. These samples were then metal coated with chromium using evaporative coating using same method as the molecular O_2 samples.

All four samples along with the test sample were loaded into the NanoESCA UHV chamber. With the test sample going first to calibrate the etch rate, the plasma etcher was used to thin an area of the chromium contact while XPS readings were regularly taken at binding energy ranges associated with chromium, oxygen, and carbon. The etch continued until the carbon XPS peak was high enough to confirm the etch pit had made it through the chromium. EF-PEEM images and UPS spectra were then taken of inside and outside the etch pit.

After being taken out of NanoESCA, the PCD ozone sample was tested using the electron gun. Probes were positioned onto the chromium and the P-type area and an IV curve was measured for an electron energy range

$0 - 20\,eV$ at an emission current of $0.01\,mA$.

4 Results and Discussion

4.1 Diode Dimensions and Features

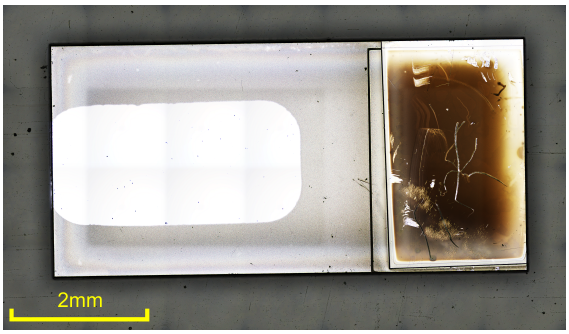

(a)

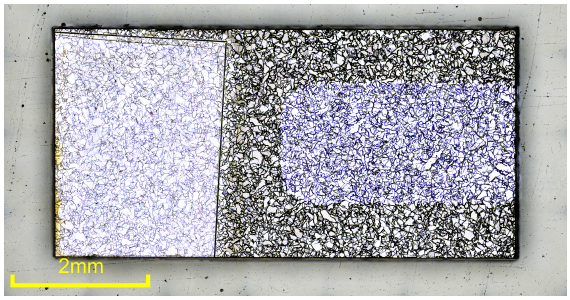

(b)

Figure 11: Top down stitched images of the (a) SCD and (b) PCD molececular O_2 samples taken before being loaded into NanoESCA.

3D LEXT scans were taken of both the molecular O_2 samples after chromium was deposited. Top down images of these scans are shown in figure 11. In the image of the SCD sample the P-type masked off area is on the right and the chromium contact is the long rectangle on the left and *vice versa* for the SCD sample. The masked off P-type area on the SCD sample is stained brown because it experienced high heat from the mask during the intrinsic diamond growth. This heat causes a thin layer of graphitic carbon to form that is brown colour. Graphitic carbon is also very soft so is easily scratched, which explains the scratches on the graphitic area in figure 11a.

For both samples the masked area is at an angle as the mask was a scrap diamond wafer balanced on the end by hand. This means that the area masked off is not consistent between samples. Near the edge of the masked off section on the SCD molecular O_2 sample there is a line indicating a ridge in the intrinsic diamond. This ridge is due to a short, failed growth of the intrinsic layer. After the growth failed the mask had to be replaced; this left a ghost of the first growth similar to double exposure on a camera.

Using the laser height map the width of the intrinsic diamond layer (as shown in figure 8b) was found by comparing the height of the masked off area and the unmasked area. The widths were found to be $6.7\,\mu m$ and $8.3\,\mu m$ for the SCD and PCD molecular O_2 samples respectively. The widths of the ozone terminated samples should be the same as their respective molecular O_2 counterparts for both SCD and PCD. This is because the two samples of the same crystal structure were paired up when growing the diamond and were always in the microwave CVD chamber at the same time. The widths of the metal layer couldn't be measured using this technique as the LEXT does not have high enough resolution to measure heights in the range of $84\,nm$, the estimated thickness of the chromium layer.

4.2 Oxygen Termination Effects

The main aim of this research was to investigate the effects of different oxygen termination techniques on two different crystal structures of diamond. Before other measurements were taken the chromium was etched away while XPS spectra were taken as described in section 2.7. The XPS intensity of the features corresponding to oxygen, chromium, and carbon over multiple etch cycles is shown in figure 12. The etch pit reaches the chromium-diamond interface when the carbon XPS signal intensity is rising and the chromium signal intensity is falling. The expectation was that the oxygen deposited during termination would stay at the chromium-diamond interface.

However, figure 12 shows that the peak oxygen intensity is reached far before the etch pit reaches the chromium-diamond interface, for all samples. This means that the oxygen was no longer at the diamond-chromium interface. The most likely reason for this is that the oxygen has migrated through the chromium due to the chromium's amorphous structure and oxidised it. Due to this the theory of oxygen termination lowering the Schottky barrier height could not be tested. This may mean that using oxygen termination for this purpose does not work, although more research needs to be undertaken to confirm this. Furthermore, it is likely that the oxygen has adversely affected the performance of the diode, as oxidised chromium will have a lower conductivity. This could be tested in future research by depositing an amorphous chromium film on oxygen terminated and unterminated diamond and then comparing the conductivity.

A weakness of this data is that the number of etch cycles are not comparable between samples, as the etch rate varied considerably between samples. Even two subsequent etches on the same sample could be at a different etch rates. Due to charging, the test sample did not provide sufficient etch rate calibration. Therefore, the etch cycle axis is in arbitrary units. This means that only general trends can be used to draw conclusions. These spectra were also analysed by taking the peak intensity for each feature and normalising the intensities to a percent for their minimum value. This along with the limited noise removal means the intensity axis is also in arbitrary units.

Figure 12 shows a low intensity carbon signal for the

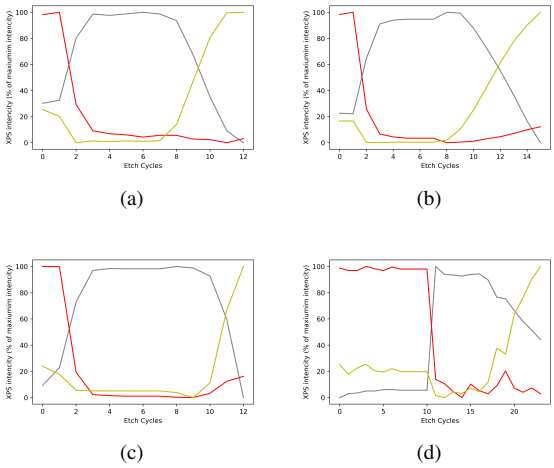

(a) (b)

(c) (d)

Figure 12: The XPS peak intensity for chromium (gray), oxygen (red), and carbon (yellow) over successive plasma etch cycles. The samples are (a) PCD molecular O_2, (b) PCD ozone, (c), SCD molecular O_2, and (d) SCD ozone.

first few etch cycles in all samples. This is from organic surface adsorbates and dust that fell onto the sample in the time between metal coating and loading into NanoESCA. The chromium signal also starts at a low intensity for all etches. Again, this is due to the effect of contamination from aforementioned surface adsorbates[76].

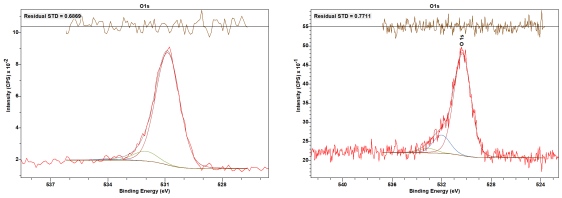

(a) (b)

Figure 13: XPS oxygen peaks for the (a) SCD molecular O_2 and (b) SCD ozone sample.

In order to confirm that the oxygen had oxidised the chromium, a more detailed analysis of the XPS spectra was undertaken as shown in figure 13. This shows the oxygen XPS peak at its highest intensity for two samples. The main oxygen peak is from a metal oxide at $530\,eV$ and there is no detectible carbonate peak. This corroborates the theory that the oxygen has completely left the chromium-diamond interface. Secondary peaks include hydroxides at $532\,eV$ and nitrates at $533\,eV$. These secondary peaks have intensities relative to the main peak of 10% and 1% for molecular O_2, and 20% and 5% for ozone. This could indicate that the molecular O_2 method creates a cleaner surface with fewer impurities than the ozone method.

It is likely that this oxidation affected data acquisition for the SCD ozone sample. In figure 12d the XPS intensity graph for the SCD ozone sample is particularly noisy and the etch rate is significantly more inconsistent than the other measurements. This is because, unlike the other samples, the SCD ozone charged from the plasma etcher. This meant that XPS readings could only be taken when the plasma etcher was off. This sample also charged when the EF-PEEM was used, meaning it was impossible to capture work function maps, Fermi level intensity maps, or UPS spectra of this sample. Therefore, after XPS no more analysis of this sample was undertaken in NanoESCA. When taken out of the NanoESCA facility, a resistance reading of this sample read as an open circuit, even up to the max setting of $200\,M\Omega$. My conclusion is that the oxygen from the ozone termination has completely saturated the chromium layer, turning it into a layer of chromium oxide and making it completely electrically insulative.

This oxidation could be a problem with future devices that use this method of chromium deposition, as they could absorb oxygen from the air and become unusable. To prevent this a possible solution could be to anneal the chromium after deposition. This will grow the crystal structure of the chromium and reduce the porosity of the metal. Further research needs to be done to confirm if this or other methods could prevent further oxidation.

4.3 EF-PEEM Data

Using NanoESCA EF-PEEM images were taken over a range of electron energies of both the diamond etch pit and the chromium. These images were processed to generate work function maps. The wide work function map in figure 14 shows the work function gradient from the diamond etch pit to the chromium and that the work function of the diamond etch pit (ϕ_d) is higher than that of the chromium (ϕ_c). This observation is confirmed by the more precise, smaller work function maps that can be seen in figure 15. From these maps it is clear that the work function of the chromium is consistently lower than the work function of the diamond underneath for all measured samples.

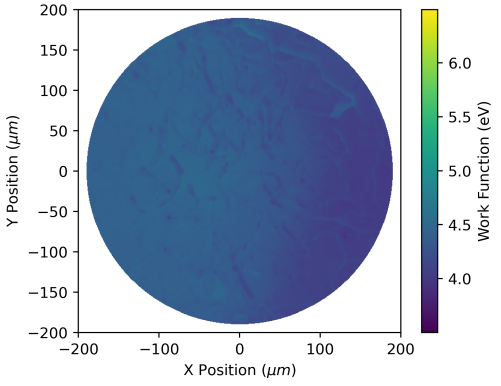

Figure 14: A wide angle work function map of the PCD molecular O_2 sample showing the gradient between the diamond etch pit on the left and chromium on the right.

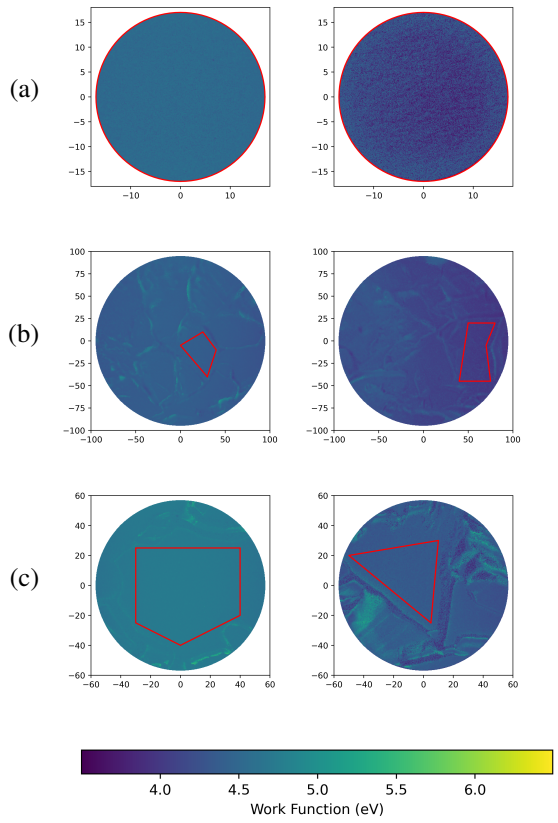

Figure 15: The work function maps of the etch pit (left) and chromium (right) for the samples (a) SCD molecular O_2, (b) PCD molecular O_2, (c) and PCD ozone. The red outline shows the areas that were averaged to find the work function.

Sample Name	$\phi_d\ (eV)$	$\phi_c\ (eV)$	$\Delta_\phi\ (eV)$
SCD mol O_2	4.54	4.14	0.40
PCD mol O_2	4.42	4.18	0.24
PCD ozone	4.73	4.33	0.40
Literature	4.15	4.60	-0.45

Table 1: Average work functions of the regions in figure 15 bordered in red, their differences, and the comparable work functions from literature. The diamond work function is from Mackie et al. [77] and the chromium work function is from Wahlin [74].

In figure 15, the work functions were found by averaging the areas bordered in red. These areas were chosen because the work function was consistent within the borders. These average values are compared with standard work function values from literature in table 1. When compared to the literature, it looks like the chromium and diamond data has been swapped, but after carefully checking all the metadata files I can confirm this data is correctly labelled[77][74]. One possible explanation for the different work function in the chromium is aforementioned oxidation from the oxygen termination diffusing into the chromium. This hypothesis is supported by research that has found that the work function of chromium can reduce by up to $1.2\,eV$ after the formation of a thick oxide layer[78].

There are three possible explanations for the differences between my measurements for diamond work functions and the diamond work function reported in literature[77]. Boron may have diffused from the P-type diamond through the intrinsic diamond layer making this diamond lightly boron doped and therefore P-type diamond. P-type diamond has a higher work function due to the lower Fermi energy[68]. Alternatively, the work function in this area may have been heavily affected by the P-type diamond underneath. The depletion region of the P-type-intrinsic junction extends far into the intrinsic material, as shown previously in section 2.6. This means that the band structure of the diamond, and therefore the work function, is bent to be same as the P-type diamond and would be almost indistinguishable from P-type diamond. Finally, the plasma etcher itself may have affected the electronic structure of the diamond, something that is discussed in detail in section 4.4.

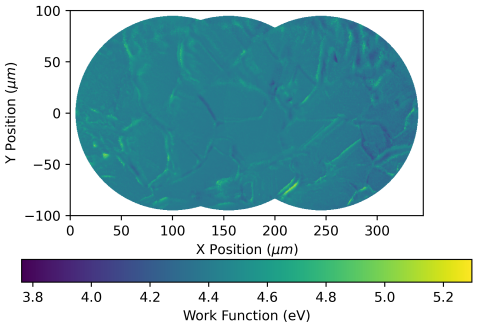

Figure 16: Multiple work function maps of the PCD molecular O_2 sample stitched together, with the diamond etch pit on the left and chromium on the right. The overlapping images allow the parabolic error in measurements to be corrected for to show a more accurate image.

The stitched image shown in figure 16 highlights an issue with work function maps of polycrystalline diamond. At the grain boundaries there are massive peaks and troughs in the work function due to the angle of the surface and shadows from the plasma etcher and UV lamp. Values for work function in specific areas can be found by averaging over a crystal face and avoiding the boundaries, as shown in figure 15. General trends are harder to show as it is challenging to separate real trends from noise. In figure 17 a Gaussian blur was applied to the graph to help with this readability challenge. Although there are still some significant spikes it shows that the work function transition between diamond and chromium is gradual.

4.4 UPS and Fermi Surface Intensity

UPS spectrums were taken at the same locations as the EF-PEEM work function maps in figure 15 for both mol-

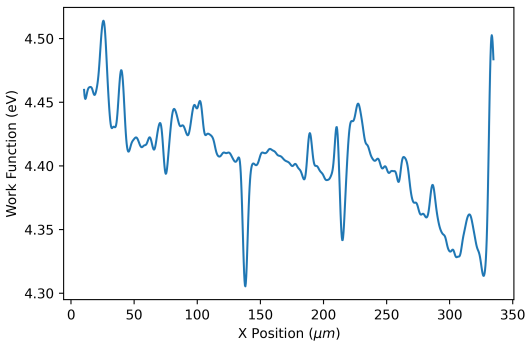

Figure 17: A one dimensional slice through the centre of figure 16 showing the work function change when moving from the diamond etch pit to the chromium. A Gaussian blur has been applied to this graph for ease of reading.

ecular O_2 samples; these spectrums are shown in figure 18. In the chromium spectrums, the Fermi edge at 0 binding energy is clearly visible. There is a peak at $\sim 1.5\,eV$, which is consistent with metallic chromium. There is also a noticeable peak at $\sim 6\,eV$; this is associated with chromium oxide and is another piece of evidence that corroborates the earlier data of oxygen diffusing into the chromium[79].

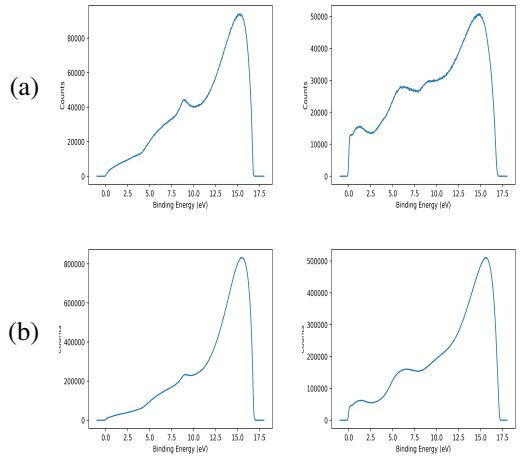

Figure 18: The UPS spectra of the etch pit (left) and chromium (right) for the samples (a) SCD molecular O_2 and (b) PCD molecular O_2 obtained when illuminated with HeI radiation ($21.22\,eV$).

The diamond UPS spectrums for both the SCD and PCD samples have very similar features. There is a peak at $\sim 8\,eV$ that has been observed in other diamond spectra[80]. The unexpected feature of these spectra is the tail stretching all the way to the Fermi level, almost looking like this diamond has Fermi edge. Although the shape is not consistent with a Fermi edge, there is a significant intensity at the Fermi level, implying that this diamond is conductive. This Fermi level intensity is also shown in figure 19, as although the intensity is much higher in chromium, there is still intensity at the Fermi level that indicate conductive materials. This Fermi intensity map also proves that the UPS tail in figure 18 is not due to left over chromium, as there is still significant Fermi surface intensity away from the grain boundaries on the crystal faces.

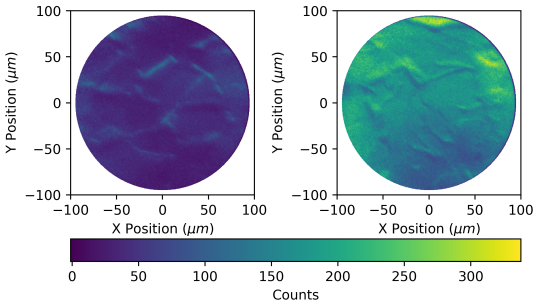

Figure 19: The Fermi surface intensity maps for the etch pit (left) and chromium (right) of the PCD molecular O_2 sample.

The initial conclusion from these results is that the plasma etcher has caused some graphitic carbon to form on the surface of the diamond and that causes the conductor-like UPS spectra. However, this was disproved by the Raman spectrum of the SCD molecular O_2 sample shown in figure 20. This spectrum shows the characteristic diamond peak at $1332\,cm^{-1}$ but no graphitic feature at $1575\,cm^{-1}$[81]. The current conclusion is that the Fermi level intensity is caused by amorphous diamond. Although the Raman spectrum is not a perfect match, the small hump at $\sim 1200\,cm^{-1}$ has been recorded before as a signature of amorphous diamond[82]. This could also be another explanation for the strange work function of the diamond as a conductive and amorphous diamond surface would have a lower Fermi level and therefore a larger work function.

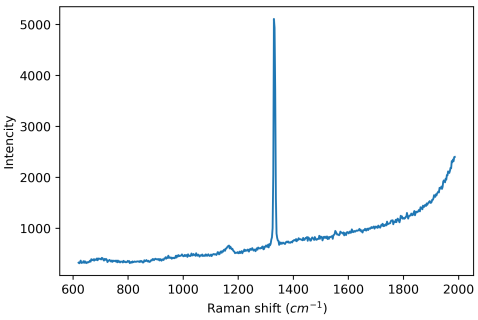

Figure 20: A Raman shift spectrum taken of the diamond inside the etch pit of the SCD molecular O_2 sample. The slow rising towards $2000\,cm^{-1}$ is caused by background level light from monitors in the room.

Irrespective of why the tails in figure 18 occur, their presence means that it is impossible to determine the Schottky barrier height from the data I have obtained.

To calculate the Schottky barrier height using XPS the position of the valance band maximum relative to the Fermi energy is required; this is found using UPS[67]. The valence band maximum in a UPS spectrum is were the lowest binding energy feature intersects the noise floor. As the diamond surface acts like a conductor after plasma etching, the valence band feature seems to be at or above the Fermi level. As this is not representative of semiconducting diamond the Schottky barrier height is unobtainable.

4.5 Carbon XPS Spectra

Once the etch pits for all samples had reached the diamond, XPS spectra were taken of the carbon peak. These are shown in figure 21. All these spectra were modelled using the semi-empirical Shirley background model and the Gaussian-Lorentzian sum peak model with the Lorentzian component set to 25%. The aforementioned charging of the SCD ozone sample meant that charge compensation was necessary. This compensation is not perfect so all the peaks for this sample are shifted down by $\sim 0.61\,eV$ and therefore this sample is not included in the following data.

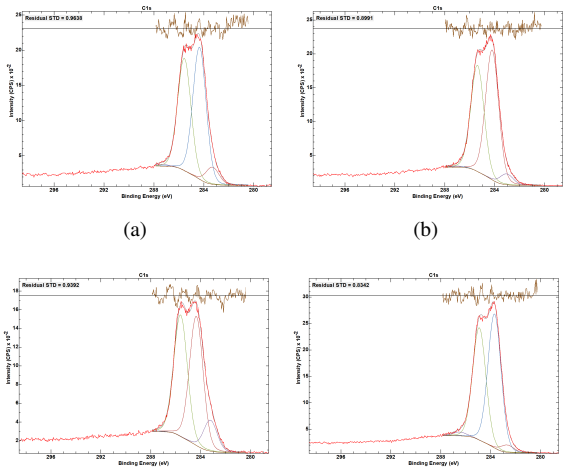

Figure 21: XPS spectra of the intrinsic diamond in the etch pit after the chromium was removed. The samples are (a) PCD molecular O_2, (b) PCD ozone, (c), SCD molecular O_2, and (d) SCD ozone.

There are two main peaks almost equal in intensity at binding energies of $\sim 284.30\,eV$ and $\sim 285.52\,eV$. These peaks have been previously identified as corresponding to sp^2 bonded carbon and sp^3 respectively [83]. The percentage ratio of sp^2:sp^3 is 54%:46%. This is more evidence indicating that the plasma etcher has created a surface of amorphous diamond. The referenced paper by Jackson and Nuzzo [83] was explicitly analysing amorphous "diamond-like" carbon when they observed these signals. In this paper, amorphous diamond was created by bombarding the surface with argon ions. This is similar to the operation of the plasma etcher used in NanoESCA where xenon ions are accelerated towards the sample to remove material. Therefore, my hypotheses that the metal-like diamond band structure originates from amorphous diamond is in line with previous research.

Two other features are present in the carbon XPS spectra. The first is a peak at $\sim 283.20\,eV$, which has an area that varies significantly between samples. This feature corresponds to chromium carbide and therefore the varying areas are probably due to differing amounts of remaining metal[84]. The second is a peak at $\sim 287.26\,eV$; a very small feature that previous research has identified as an sp^2 satellite peak but could also be from nitrogen contamination[83, 85].

4.6 Power Generation

The power generating capabilities of the PCD ozone sample as a betavoltaic cell were tested using the electron gun. By setting the election energy and current it is possible to simulate exposure to beta particle emitting radioactive sources and estimate the electronic response. The I-V curves during these tests are shown in figure 22. There is a clearly asymmetric current response to voltage showing that the device is acting as a diode, although this response seems to lessen once electron beam energy increases. The difference between the maximum and minimum current also increases, which indicates a lower resistance for the ohmic component of the curve.

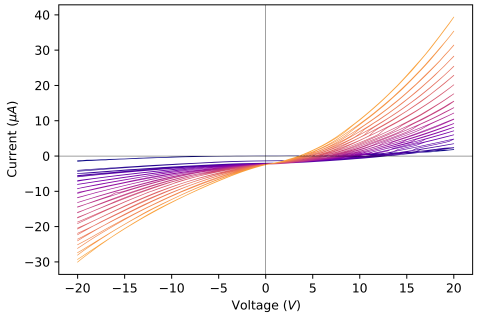

Figure 22: The I-V curves of the PCD ozone betavoltaic cell when being exposed to an electron beam emitting $0.01\,mA$ of electrons at energies ranging from $0\,eV$ (blue) to $20\,eV$ (yellow).

The actual power generated by the cell is shown in figure 23. The peak power generation quickly rises to $\sim 9\,\mu W$ at $2\,eV$ but then steadily decreases. This is unexpected, as a higher electron energy should create more electron hole pairs. Higher energy electrons will have a higher penetration depth, which could mean the electrons pass through the intrinsic diamond and deposit their energy in the P-type diamond underneath. However, this does not seem feasible as computational modelling of the electron gun indicates the $6\,\mu m$ thick intrinsic layer is sufficient to absorb electrons up to $20\,eV$.

A hint of the most likely reason for reduced power at higher electron energies can be seen in figure 23a.

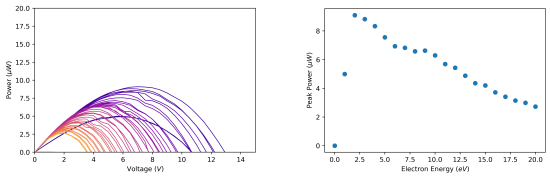

(a) (b)

Figure 23: (a) The P-V curves of the PCD ozone betavoltaic cell when being exposed to an electron beam emitting $0.01\,mA$ of electrons at energies ranging from $0\,eV$ (blue) to $20\,eV$ (yellow), focused on the ranges where energy is generated. (b) The peak powers of the data shown in part subfigure (a) over the same range.

The power curves for higher electron energies are initially the same as their lower energy counterparts, but the higher energy curves start reducing in power at lower voltages. This indicates that there is a similar production of electron hole pairs, but the rectifying ability of the diode is reduced. This would explain the reducing asymmetry of figure 22 as electron energy increases. This would also explain the lower resistance of the diode's ohmic region, as the less diode-like the device is, the more conductive it is.

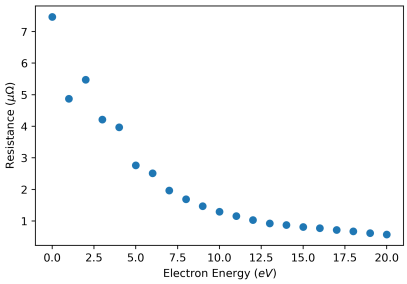

Figure 24: The estimated resistances for the PCD ozone betavoltaic cell when exposed to different energy electron beams at an emission current of $0.01\,mA$. These resistances were found by taking the gradients of the I-V curves in figure 22 between $-20\,V$ and $-15\,V$.

All this evidence combined would indicate the reason the cell is acting less diode-like is because it is heating up. As the temperature of the diode increases, more of the boron accepters in the P-type diamond get ionised and if enough are ionised the diamond's conduction will be metal-like. This means the diode is becoming a regular, symmetrical conductor as it heats up. This is corroborated by the graph of resistances at varying electron energies shown in figure 24, demonstrating that the resistance has an inverse exponential relationship to the electron energy. Because the current carrier density has an exponential relationship with temperature (as shown in equation 2) and the resistivity is inversely proportional to carrier density, resistance should have an inverse exponential relationship to temperature and therefore electron energy. This simple model matches up with the trend shown in figure 24.

This relationship between temperature and power generation is unlikely to be a problem with these devices when in use. When testing with the electron gun, the sample is in a vacuum chamber with very little way for heat to dissipate from the sample. In real world applications the diode would to be cooled by ambient air, while in high temperatures applications lower dopant levels can be used. It could also be possible that lower dopant levels would lead to higher efficiency at ambient temperatures, but more research in this area needs to be done to test this theory.

To prove this theory, temperature sensors could be added to the inside of the electron gun chamber. This would confirm whether the temperature of the diode is increasing. If the diode is indeed heating up cooling could be added to the electron gun platform to make temperature a controlled variable and test if it is causing the reduction in rectification.

5 Conclusion

The original goal of this project was to investigate possible efficiency improvements in diamond betavoltaic cells by terminating the diamond with oxygen to reduce the Schottky barrier height for electrons. Two different oxygen termination methods were used for comparison. The discovery oxygen easily diffuses through chromium when deposited with evaporative deposition meant that neither method was found to be effective. Furthermore, oxidised chromium could reduce the efficiency of the cell because of it's low conductivity. Although these results need to be confirmed with future research, my results would suggest that this method for reducing Schottky barrier height is ineffective and other avenues should be explored. Further research also needs to be undertaken to prevent chromium from oxidising when exposed to the atmosphere. It is possible that annealing the chromium immediately after deposition would reduce its amorphous character and therefore oxidation.

My work function results (table 1) show that the work function of the diamond in my devices was greater than the work function of the chromium. This is inconsistent with previous research and I have discussed a few different theories as to why this might be the case. More research needs to be done to determine why the apparent work functions are different from published literature. However, This is of lower importance as I believe that research into the other unanswered questions in this report will link back to this anomaly.

I found that characterizing polycrystalline diamond films in the NanoESCA facility is challenging due to anomalies at the grain boundaries. When performing future research this could be mitigated by focusing on single crystal devices and creating automated tools for filtering out the noise at grain boundaries.

The main observation that requires future investigation is the strange conductivity of the diamond etched area. Not knowing what is causing this effect could negatively

impact the performance of future devices. Unexpectedly high conductivity in diamond could also hinder future research by causing faulty or failed measurements. Focused research into the phenomenon is required to prevent this and there could be many benefits to being able to control the effect. Highly conductive diamond might even open up opportunities for new, unthought-of devices.

A particularly intriguing observation was the effect of electron energy on betavoltaic power generation. I observed that the higher the electron energy, the lower the diode's rectification. This reduction of rectification hampered the current generation at higher voltages. This, in combination with the reduction in resistance, leads me to hypothesise that the higher electron energies are heating up the diode. The diode cannot dissipate this heat as it is in a vacuum chamber and is thermally isolated from the outside. An increased temperature would ionise more of the boron accepters in the P-type diamond, thus reducing the built-in voltage and the diode's rectification.

If confirmed, this would be a very important result given that many diamond-based electrical devices are planned to be incorporated into spacecraft or fusion reactors, environments with wide ranging and high temperatures. This could also have major implications for future betavoltaic cell designs. The significance of the drop in performance might also signify lower dopant densities could increase rectification even at lower temperatures. I am excited about the possibility of future research investigating some of the unanswered questions raised in this report and how my findings could affect future devices.

Appendices

Acronym List

- XPS – X-ray Photoelectron Spectroscopy
- SBH – Schottky Barrier Height
- UPS – UV Photoelectron Spectroscopy
- RTG – Radioisotope Thermoelectric Generator
- PCD – Polycristaline Diamond
- SCD – Single Crysal Diamond
- PIM – P-Type Intrinsic Metal
- PIN – P-Type Intrinsic N-Type
- MEMS – Micro Electrical Mechanical Systems
- BDD – Boron Doped Diamond
- UV – Ultra Violet
- GPS – Global Positioning System
- UVC – UV light in the C energy band of 100–$280\,nm$
- PN – P-Type N-Type
- CVD – Chemical Vapour Deposition
- HPHT – High Pressure High Temperature
- UHV – Ultra High Vaccume
- EF-PEEM – Energy-Filtered Photoelectron Emission Microscopy

Symbol List

- E_g – Semiconductor Band Gap
- E_D – Electron Donor Energy Level
- E_A – Electron Accepter Energy Level
- N_D^+ – Ionised Donor Density
- N_A^- – Ionised Accepter Density
- N_D – Donor Density
- N_A – Accepter Density
- T – Temperature
- k_b – Boltzmann's Constant
- E_F – Fermi energy
- g – Ground State Degeneracy
- n – Intrinsic Negative Charge Carrier Density
- p – Intrinsic Positive Charge Carrier Density
- N_C – Density of states in the Conduction Band
- N_V – Density of states in the Valence Band
- E_C – Energy Level at the bottom of the Conduction Band
- E_V – Energy Level at the top of the Valence Band
- x_n – Depletion Width in an N-Type Semiconductor
- x_p – Depletion Width in a P-Type Semiconductor
- q – The Charge of an Electron
- ϵ_s – The Permittivity of a Semiconductor
- V_bi – Built-In Voltage
- ζ_n – $E_V - E_F$ in an N-Type Semiconductor
- ζ_p – $E_F - E_C$ in a P-Type Semiconductor
- ϕ_n – The Work Function of an N-Type Semiconductor
- ϕ_p – The Work Function of a P-Type Semiconductor

- χ_n – The Electron Affinity of an N-Type Semiconductor
- χ_p – The Electron Affinity of a P-Type Semiconductor
- ϕ_m – The Work Function of a metal
- ϕ_B – The Schottky Barrier Height
- E_{vac} - Energy Level of the Vacuum
- ϕ_i – The Work Function of an Intrinsic Semiconductor
- χ_i – The Electron Affinity of an Intrinsic Semiconductor
- ζ_i – $E_V - E_F$ in an Intrinsic Semiconductor
- ϕ_i – The Work Function of an Intrinsic Semiconductor with Oxygen Termination
- χ_i – The Electron Affinity of an Intrinsic Semiconductor with Oxygen Termination
- x_i – Depletion Width in an Intrinsic Semiconductor

References

[1]W. Raza, F. Ali, N. Raza, Y. Luo, K.-H. Kim, J. Yang, S. Kumar, A. Mehmood, and E. E. Kwon, "Recent advancements in supercapacitor technology", Nano Energy **52**, 441–473 (2018).

[2]N. T. Balakrishnan, A. Das, N. Jishnu, L. R. Raphael, J. D. Joyner, J.-H. Ahn, M. Jabeen Fatima, and R. Prasanth, "The great history of lithium-ion batteries and an overview on energy storage devices", Electrospinning for Advanced Energy Storage Applications, 1–21 (2021).

[3]J. Lach, K. Wróbel, J. Wróbel, P. Podsadni, and A. Czerwiński, "Applications of carbon in lead-acid batteries: a review", Journal of Solid State Electrochemistry **23**, 693–705 (2019).

[4]N. Kittner, O. Schmidt, I. Staffell, and D. M. Kammen, "Grid-scale energy storage", in *Technological learning in the transition to a low-carbon energy system* (Elsevier, 2020), pp. 119–143.

[5]J. Blanchard, "The unlikely revival of nuclear batteries: startups plan to put them in robots, sensors, and medical implants", IEEE Spectrum **62**, 42–48 (2025).

[6]S. Toledo, "Evaluating batteries for advanced wildlife telemetry tags", IET Wireless Sensor Systems **5**, 235–242 (2015).

[7]V. S. Mallela, V Ilankumaran, and N. Rao, "Trends in cardiac pacemaker batteries", Indian pacing and electrophysiology journal **4**, 201 (2004).

[8]S. Fruitsmaak, *Artificial pacemaker victory sr 5610, removed from a deceased patient before cremation.* Tech. rep. (`https://commons.wikimedia.org/w/index.php?curid=2909069`, 2007).

[9]Abbott, *Product performance report: 2025 first edition*, tech. rep. (Abbott group, 2025).

[10]E. W. Lau, "Technologies for prolonging cardiac implantable electronic device longevity", Pacing and Clinical Electrophysiology **40**, 75–96 (2017).

[11]R. Rudd, J. Hall, and G. Spradlin, "The voyager interstellar mission", Acta astronautica **40**, 383–396 (1997).

[12]U. D. of Energy, "What is a radioisotope power system?", in Https://www.energy.gov/ne/articles/what-radioisotope-power-system (2021).

[13]G. Fradkin and V. Kodyukov, "Radioisotope thermoelectric generators", Soviet Atomic Energy **26**, 193–198 (1969).

[14]R. O'brien, R. Ambrosi, N. Bannister, S. Howe, and H. V. Atkinson, "Safe radioisotope thermoelectric generators and heat sources for space applications", Journal of Nuclear Materials **377**, 506–521 (2008).

[15]H. Salh, "Improving the overall efficiency of radioisotope thermoelectric generators", Advances in Energy and Power **2**, 21–26 (2014).

[16]J. E. Werner, S. G. Johnson, C. C. Dwight, and K. L. Lively, *Cost comparison in 2015 dollars for radioisotope power systems–cassini and mars science laboratory*, tech. rep. (Idaho National Laboratory (INL), Idaho Falls, ID (United States), 2016).

[17]Deglr6328, *Radioisotope thermoelectric generator plutonium pellet*, tech. rep. (`https://commons.wikimedia.org/w/index.php?curid=11198885`, 2005).

[18]C. Zhou, J. Zhang, X. Wang, Y. Yang, P. Xu, P. Li, L. Zhang, Z. Chen, H. Feng, and W. Wu, "Betavoltaic cell: the past, present, and future", ECS Journal of Solid State Science and Technology **10**, 027005 (2021).

[19]A. Krasnov and S. Legotin, "Advances in the development of betavoltaic power sources (a review)", Instruments and Experimental Techniques **63**, 437–452 (2020).

[20]L. Partain, "Solar cell device physics", Solar cells and their applications, 67–109 (2010).

[21]C. M. Bourget, "An introduction to light-emitting diodes", HortScience **43**, 1944–1946 (2008).

[22]L. C. Olsen, P. Cabauy, and B. J. Elkind, "Betavoltaic power sources", Physics today **65**, 35–38 (2012).

[23]G. W. Crabtree and N. S. Lewis, "Solar energy conversion", Physics today **60**, 37–42 (2007).

[24]H. Guo and A. Lal, "Nanopower betavoltaic microbatteries", in Transducers'03. 12th international conference on solid-state sensors, actuators and microsystems. digest of technical papers (cat. no. 03th8664), Vol. 1 (IEEE, 2003), pp. 36–39.

[25]E. B. Yakimov, "Prediction of betavoltaic battery parameters", Energies **16**, 3740 (2023).

[26]M. B. Naseem, H. S. Kim, J. Lee, C. H. Kim, and S.-I. In, "Betavoltaic nuclear battery: a review of recent progress and challenges as an alternative energy source", The Journal of Physical Chemistry C **127**, 7565–7579 (2023).

[27]E. B. Agyekum, "Beta-voltaic nuclear batteries–review of recent developments, challenges and future research directions", Journal of Energy Storage **122**, 116701 (2025).

[28]"U-blox m10: ultra-low power gps for small, high-performance trackers and wearables", in Tech (u-blox, 2020).

[29]J. Dixon, A. Rajan, S. Bohlemann, D. Coso, A. D. Upadhyaya, A. Rohatgi, S. Chu, A. Majumdar, and S. Yee, "Evaluation of a silicon 90sr betavoltaic power source", Scientific reports **6**, 38182 (2016).

[30]V. Chepurnov, M. Dolgopolov, O. Kuznetsov, and G. Puzyrnaya, "Optimization of the beta converter", 22.251 431+ 95.4 341, 368 (2019).

[31]M Kovari, M Coleman, I Cristescu, and R Smith, "Tritium resources available for fusion reactors", Nuclear Fusion **58**, 026010 (2018).

[32]K. Fu, M. Chen, S. Wei, and X. Zhong, "A comprehensive review on decontamination of irradiated graphite waste", Journal of Nuclear Materials **559**, 153475 (2022).

[33]D. for Energy Security and N. Zero, "Scope of and exemptions from the radioactive substances legislation in england, wales and northern ireland", in Guidance document (2024).

[34]T. E. Adams and S. T. Revankar, "Research, development, and evaluation capabilities for betavoltaic power sources", in 2015 asee annual conference & exposition (2015), pp. 26–1334.

[35]V. S. Vavilov and E. A. Konorova, "Semiconducting diamonds", Soviet Physics Uspekhi **19**, 301 (1976).

[36]J. Custers, "Unusual phosphorescence of a diamond", Physica **18**, 489–496 (1952).

[37]R. Kalish, "Doping of diamond", Carbon **37**, 781–785 (1999).

[38]W Saslow, T. Bergstresser, and M. L. Cohen, "Band structure and optical properties of diamond", Physical Review Letters **16**, 354 (1966).

[39]international standards organisation, "Iso 21348 definitions of solar irradiance spectral categories", in Space environment (natural and artificial) (2007).

[40]F. T. Porter, "Beta decay energy of tritium", Physical Review **115**, 450 (1959).

[41]C. S. Cook, L. M. Langer, and H. C. Price Jr, "Study of the beta-spectra of c 14 and s 35", Physical Review **74**, 548 (1948).

[42]C Bauer, I Baumann, C Colledani, J Conway, P Delpierre, F Djama, W Dulinski, A Fallou, K. Gan, R. Gilmore, et al., "Radiation hardness studies of cvd diamond detectors", Nuclear Instruments and Methods in Physics Research Section A: Accelerators, Spectrometers, Detectors and Associated Equipment **367**, 207–211 (1995).

[43]W. De Boer, J. Bol, A. Furgeri, S. Müller, C. Sander, E. Berdermann, M. Pomorski, and M. Huhtinen, "Radiation hardness of diamond and silicon sensors compared", physica status solidi (a) **204**, 3004–3010 (2007).

[44]J. E. Field, *The properties of natural and synthetic diamond* (Academic Press, 1992).

[45]K. Fu, M. Chen, S. Wei, and X. Zhong, "A comprehensive review on decontamination of irradiated graphite waste", Journal of Nuclear Materials **559**, 153475 (2022).

[46]L. Fuks, I. Herdzik-Koniecko, K. Kiegiel, and G. Zakrzewska-Koltuniewicz, "Management of radioactive waste containing graphite: overview of methods", Energies **13**, 4638 (2020).

[47]M. Li, D. Yu, S. Shen, and X. Liu, "Review of n-type doping diamond: methods, elements, and properties", Carbon Letters **35**, 1981–2009 (2025).

[48]R. Kalish, "Doping of diamond", Carbon **37**, 781–785 (1999).

[49]S Koizumi, M Kamo, Y Sato, S Mita, A Sawabe, A Reznik, C Uzan-Saguy, and R Kalish, "Growth and characterization of phosphorus doped n-type diamond thin films", Diamond and related materials **7**, 540–544 (1998).

[50]M. T. Islam and H. Efeoglu, "Temperature-dependent i–v characteristics of schottky diodes: a comprehensive review of barrier height, ideality factor, and series resistance", Journal of Electronic Materials, 1–34 (2025).

[51]V. Grushko, O. Beliuskina, A. Mamalis, V. Lysakovskiy, E. Mitskevich, A. Kiriev, E. Petrosyan, R. Chaplynskyi, O. Bezshyyko, and O. Lysenko, "Energy conversion efficiency in betavoltaic cells based on the diamond schottky diode with a thin drift layer", Applied Radiation and Isotopes **157**, 109017 (2020).

[52]S. M. Sze, Y. Li, and K. K. Ng, *Physics of semiconductor devices*, 3rd ed. (John Wiley & Sons, 2012).

[53]W. Shockley, "The theory of p-n junctions in semiconductors and p-n junction transistors", Bell system technical journal **28**, 435–489 (1949).

[54]L. Lin, R. Jacobs, T. Ma, D. Chen, J. Booske, and D. Morgan, "Work function: fundamentals, measurement, calculation, engineering, and applications", Physical Review Applied **19**, 037001 (2023).

[55]M. C. Day, M. G. Pamato, D. Novella, and F. Nestola, "Imperfections in natural diamond: the key to understanding diamond genesis and the mantle", La Rivista del Nuovo Cimento **46**, 381–471 (2023).

[56]U. F. D'Haenens-Johansson, J. E. Butler, and A. N. Katrusha, "Synthesis of diamonds and their identification", Reviews in Mineralogy and Geochemistry **88**, 689–753 (2022).

[57]C. E. Nebel, "Cvd diamond: a review on options and reality", Functional Diamond **3**, 2201592 (2023).

[58]B. Dischler, "Cvd diamond: a new and promising material", in *Low-pressure synthetic diamond: manufacturing and applications*, edited by B. Dischler and C. Wild (Springer Berlin Heidelberg, Berlin, Heidelberg, 1998), pp. 3–7.

[59]P. W. May, "Diamond thin films: a 21st-century material", Philosophical Transactions of the Royal Society of London. Series A: Mathematical, Physical and Engineering Sciences **358**, 473–495 (2000).

[60]J. Creighton and P Ho, "Introduction to chemical vapor deposition (cvd)", ASM International **407** (2001).

[61]W. G. Eversole, "Diamond synthesis", US patents **3030188** (1962).

[62]B. Derjaguin, D. Fedoseev, V. Lukyanovich, B. Spitzin, V. Ryabov, and A. Lavrentyev, "Filamentary diamond crystals", Journal of Crystal Growth **2**, 380–384 (1968).

[63]D. J. Poferl, N. C. Gardner, and J. C. Angus, "Growth of boron-doped diamond seed crystals by vapor deposition", Journal of Applied Physics **44**, 1428–1434 (1973).

[64]S. M. Leeds, "Characterisation of the gas-phase environment in a microwave plasma enhanced diamond chemical vapour deposition reactor using molecular beam mass spectrometry", PhD thesis (University of Bristol, 1999).

[65]K. Kobashi, K. Nishimura, Y. Kawate, and T. Horiuchi, "Synthesis of diamonds by use of microwave plasma chemical-vapor deposition: morphology and growth of diamond films", Physical review B **38**, 4067 (1988).

[66]E. Dobročka and J. Osvald, "Influence of barrier height distribution on the parameters of schottky diodes", Applied Physics Letters **65**, 575–577 (1994).

[67]R. T. Tung, "The physics and chemistry of the schottky barrier height", Applied Physics Reviews **1**, 011304 (2014).

[68]O Romanyuk, I Bartoš, I Gordeev, A Artemenko, M Varga, T Ižák, M Marton, P Jiříček, and A Kromka, "Electron affinity of undoped and boron-doped polycrystalline diamond films", Diamond and Related Materials **87**, 208–214 (2018).

[69]R. Zulkharnay, G. Zulpukarova, and P. W. May, "Oxygen-terminated diamond: insights into the correlation between surface oxygen configurations and work function values", Applied Surface Science **658**, 159776 (2024).

[70]R. Zulkharnay, W. Greenwood, A. Wood, J. Laverock, and N. A. Fox, "Achieving a large net 'negative electron affinity' on diamond (100) via molecular oxygen and lithium functionalization", Preprint paper.

[71]R. Kravets, M. Vanecek, C. Piccirillo, A. Mainwood, and M. Newton, "A quantitative study of the boron acceptor in diamond by fourier-transform photocurrent spectroscopy", Diamond and Related Materials **13**, 1785–1790 (2004).

[72]loffe Institute, "Diamond band structure and carrier concentration", in `\NoCaseChange{www.ioffe.ru/SVA/NSM/Semicond/Diamond/bandstr.html}` (Accessed May 2026).

[73]K. E. Spear and J. P. Dismukes, *Synthetic diamond: emerging cvd science and technology* (John Wiley & Sons, 1994).

[74]H. B. Wahlin, "The thermionic properties of chromium", Physical review **73**, 1458 (1948).

[75]C. Brendel, "Topologically protected transport of phonons at the nanoscale", PhD thesis (Jan. 2019), p. 89.

[76]G. C. Smith, "Evaluation of a simple correction for the hydrocarbon contamination layer in quantitative surface analysis by xps", Journal of electron spectroscopy and related phenomena **148**, 21–28 (2005).

[77]W. Mackie, J. E. Plumlee, and A. Bell, "Work function measurements of diamond film surfaces", Journal of Vacuum Science & Technology B: Microelectronics and Nanometer Structures Processing, Measurement, and Phenomena **14**, 2041–2045 (1996).

[78]G Gewinner, J. Peruchetti, A Jaegle, and A Kalt, "Photoemission study of the chromium (111) surface interacting with oxygen", Surface science **78**, 439–458 (1978).

[79]D Gall, R Gampp, H. Lang, and P Oelhafen, "Pulsed plasma deposition of chromium oxide/chromium-cermet coatings", Journal of Vacuum Science & Technology A: Vacuum, Surfaces, and Films **14**, 374–379 (1996).

[80]S. Torrengo, L. Minati, M. Filippi, A. Miotello, M. Ferrari, A. Chiasera, E. Vittone, A Pasquarelli, M Dipalo, E Kohn, et al., "Xps and ups investigation of the diamond surface oxidation by uv irradiation", Diamond and related materials **18**, 804–807 (2009).

[81]S. Solin and A. Ramdas, "Raman spectrum of diamond", Physical Review B **1**, 1687 (1970).

[82]S Prawer, K. Nugent, and D. Jamieson, "The raman spectrum of amorphous diamond", Diamond and Related Materials **7**, 106–110 (1998).

[83]S. T. Jackson and R. G. Nuzzo, "Determining hybridization differences for amorphous carbon from the xps c 1s envelope", Applied Surface Science **90**, 195–203 (1995).

[84]M Detroye, F Reniers, C Buess-Herman, and J Vereecken, "Aes–xps study of chromium carbides and chromium iron carbides", Applied Surface Science **144-145**, 78–82 (1999).

[85]J. F. Moulder, W. F. Stickle, P. E. Sobol, and K. D. Bomben, *Handbook of x-ray photoelectron spectroscopy: a reference book of standard spectra for identification and interpretation of xps data* (Perkin-Elmer Corporation, 1992).

Certification of ownership of the copyright

This Project Report is presented as part of, and in accordance with, the requirements for the degree of MSci at the University of Bristol, Faculty of Science.

I hereby assert that I own exclusive copyright in the item named below. I give permission to the University of Bristol Library to add this item to its stock and to make it available for consultation in the library, and for inter-library lending for use in another library. I also give consent for this report to made available electronically to staff and students within the University of Bristol. It may be copied in full or in part for any bona fide library or research work. No quotation and no information derived from it may be published without the author's prior consent.

Author	Thomas Botwood
Title	Functionalised Diamond Surfaces.
Date of submission	13/04/26

I agree that submission of this report constitutes signing of this declaration.

This project/dissertation is the property of the University of Bristol and may only be used with due regard to the rights of the author. Bibliographical references may be noted, but no part may be copied for use or quotation in any published work without the prior permission of the author. In addition, due acknowledgement for any use must be made.